ELSEVIER

Advances in Colloid and Interface Science 120 (2006) 47–56

ADVANCES IN COLLOID AND INTERFACE SCIENCE

www.elsevier.com/locate/cis

Characterization of zero-valent iron nanoparticles

Yuan-Pang Sun [a], Xiao-qin Li [a], Jiasheng Cao [a], Wei-xian Zhang *, H. Paul Wang [b]

[a] *Center for Advanced Materials and Nanotechnology, Department of Civil and Environmental Engineering, Lehigh University, Bethlehem, PA 18015, United States*
[b] *Department of Environmental Engineering, National Cheng Kung University, Tainan City 70101, Taiwan*

Available online 12 May 2006

Abstract

The iron nanoparticle technology has received considerable attention for its potential applications in groundwater treatment and site remediation. Recent studies have demonstrated the efficacy of zero-valent iron nanoparticles for the transformation of halogenated organic contaminants and heavy metals. In this work, we present a systematic characterization of the iron nanoparticles prepared with the method of ferric iron reduction by sodium borohydride. Particle size, size distribution and surface composition were characterized by transmission electron microscopy (TEM), X-ray diffraction (XRD), high-resolution X-ray photoelectron spectroscopy (HR-XPS), X-ray absorption near edge structure (XANES) and acoustic/electroacoustic spectrometry. BET surface area, zeta (ζ) potential, iso-electric point (IEP), solution Eh and pH were also measured. Methods and results presented may foster better understanding, facilitate information exchange, and contribute to further research and development of iron nanoparticles for environmental and other applications.

Keywords: Zero-valent iron; Nanoparticles; Transmission electron microscopy; X-ray photoelectron spectroscopy; Surface charge

Contents

* Corresponding author.
E-mail address: wez3@lehigh.edu (W. Zhang).

0001-8686/$ - see front matter © 2006 Elsevier B.V. All rights reserved.
doi:10.1016/j.cis.2006.03.001

1. Introduction

Nanotechnology is the engineering and art of manipulating matter at the nanoscale (1–100 nm) [1–3]. For environmental applications, nanotechnology offers the potential of novel functional materials, processes and devices with unique activity toward recalcitrant contaminants, enhanced mobility in environmental media and desired application flexibility [3–10]. Many nano-based environmental technologies (e.g., sensors, sorbents, reactants) are under very active research and development, and are expected to emerge as the next generation environmental technologies to improve or replace various conventional environmental technologies in the near future [3–10].

Iron nanoparticle technology represents perhaps one of the first generation nanoscale environmental technologies [4]. Over the last few years, various synthetic methods have been developed to produce iron nanoparticles [3,4,11–14], modify the nanoparticle surface properties [15–19], and enhance the efficiency for field delivery and reactions [17–20]. Extensive laboratory studies have demonstrated that nanoscale iron particles are effective for the transformation of a wide array of common environmental contaminants such as chlorinated organic solvents [3,4,17,19,21,22], organochlorine pesticides [23], PCBs [3,24], organic dyes [25], various inorganic compounds [26,27] and metal ions such as As(III), Pb(II), Cu (II), Ni(II) and Cr(VI) [16,26,28]. Several field tests have demonstrated the promising prospective for in situ remediation [19,29,30].

Many research papers on applications of iron nanoparticles have been published over the last few years. While several types of iron nanoparticles are available on the market, information on the nanoparticle synthesis and properties is still limited in peer-reviewed journals. Fundamental information on characterization methods has not been well documented. Quality control and insurance is rapidly becoming a major issue as nanoparticles are being used in more and more projects. Objective of this work is to provide an in-depth report on the characterization of zero-valent iron nanoparticles. The synthetic methods described in this work have been used in many laboratories. We believe that such information is valuable for the comparison and quality control of iron nanoparticles produced with different methods and experimental conditions.

2. Experimental methods

2.1. Synthesis of iron nanoparticles

Nanoscale zero-valent iron particles can be prepared in aqueous solutions via the reduction of ferric iron (Fe(III)) or ferrous iron(II) with sodium borohydride [3,4], or via decomposition of iron pentacarbonyl ($Fe(CO)_5$) in organic solvents or in argon [11,12,13]. Zero-valent iron particles can also be prepared from hydrogen reduction of iron oxides. In this work, synthesis of nanoscale iron particles with the sodium borohydride method was used. A key advantage of this method is its simplicity. It can be safely done in most chemistry lab with simple chemical reagents. Specifically, the synthesis of iron nanoparticles was conducted in a flask reactor with three open necks as illustrated in Fig. 1. The central neck was housed with a tunable mechanical stirrer at 400 rpm. Through titration at a rate of 0.625 mL/s, the borohydride was introduced to reduce ferric ion (Fe^{3+}) to zero-valent iron [Fe^0], according to the following reaction:

$$4Fe^{3+} + 3BH_4^- + 9H_2O \rightarrow 4Fe^0\downarrow + 3H_2BO_3^- + 12H^+ + 6H_2 \quad (1)$$

Typically, 1:1 volume ratio of $NaBH_4$ (0.2 M) and $FeCl_3 \cdot 6H_2O$ (0.05 M) were vigorously mixed in the flask reactor for additional 30 min after the titration. Note that complete reduction of 0.05 mol Fe^{3+} requires only 0.0375 mol of BH_4^-. The excessive borohydride (0.2 M) was applied to accelerate the synthesis reaction. Experimental parameters such as pH, reactant concentrations, stirring speed, titration rate, reaction time and external temperature (23 ± 0.5 °C) can, to some extent, influence the composition and surface properties of produced iron particles and hence need to be maintained constant in the experiments to produce consistent samples. The generated iron particles were harvested with vacuum filtration and stabilized with a large volume of deionized water (> 100 mL/g) to wash, and at the end, with diluted ethanol (~ 5%). For storage, our experience suggests that maintaining a thin layer of ethanol on the top of iron particles can help preserve the nanoparticles.

2.2. Characterizations

2.2.1. Transmission electron microscopy (TEM)

Images of iron nanoparticles were recorded with a Philips EM 400T Transmission Electron Microscopy (TEM) (Philips Electronics Co., Eindhoven, Netherlands) operated at 100 kV. Samples were prepared by depositing two to three droplets of dilute ethanol solution of the nanoparticles onto a carbon film (Ernest Fullam Inc., Latham, NY). The samples were then put in a vacuumed hood till the ethanol was evaporated completely.

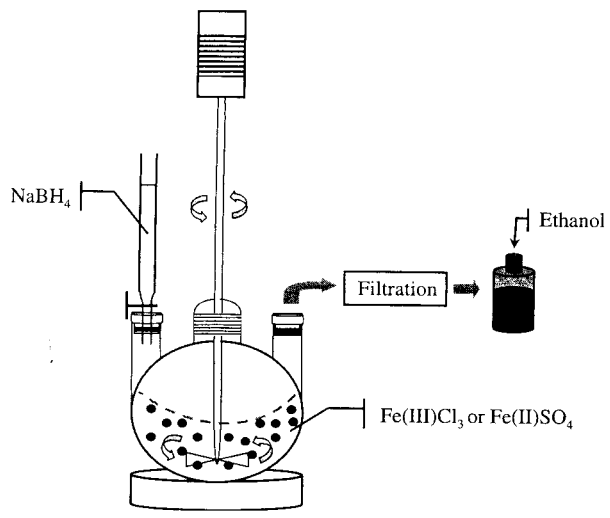

Fig. 1. Experimental setup for iron nanoparticle synthesis.

2.2.2. Size and size distribution

The particle size and size distribution were measured with an Acoustic Spectrometer (DT 1200, Dispersion Technology Inc., Bedford Hills, NY), which utilizes the sound pulses transmitted through a particle suspension to measure the properties of suspended particles. Based on the combined effect of absorption and scattering of acoustic energy, an acoustic sensor measures attenuation frequency spectra in the sample. The sensor utilizes two identical piezoelectric transducers, separated by an adjustable gap that is controlled by a stepping motor. The gap between the transmitter and receiver can be adjusted in steps. In default, the gap changes from 0.15 mm up to 20 mm in 21 logarithmic steps. The basic frequency of pulse changes in steps at the same time. The frequency changes, in default, from 3 to 100 MHz in 18 logarithmic steps. The number of pulses collected for the each gap and frequency step is automatically adjusted to reach a target signal-to-noise ratio. An analysis program calculating the particle size distribution (PSD) from attenuation spectra has been developed by the manufacturer. This program automatically searches the best-fit PSD and tests normal, log-normal and bimodal particle size distributions [31,32].

The Acoustic Spectrometer was connected to a four-neck 500-mL flask reactor in which the iron nanoparticles (1–10 g/L) were suspended in deionized (DI) water (Fig. 2). The center neck was used to house a mechanical stirrer with tunable speeds. Two of side necks were connected to the sample chamber of the acoustic spectrometer, forming a closed recirculation loop. During the measurement, the flask reactor was also purged with high purity nitrogen gas and submersed in a water bath to maintain a constant temperature (22±1 °C) in the reactor as a stable temperature is desired for minimizing the temperature effect on acoustic attenuation frequency. The remaining open neck was used as an injection port by which acid or base solution was introduced for the ζ potential titration experiment.

Compared to traditional light scattering techniques, the acoustic method is relatively flexible with no limitation on opaque materials and can measure dynamic particles in flowing systems [33]. A single particle size measurement can be rapidly completed in less than 8 min. The size range is from 5 nm to 1000 μm. For high precision, a particle concentration of at least >1 wt.% is suggested. In addition, no calibration with the known particle size is needed [32].

2.2.3. BET surface area

Specific surface area of the nanoparticle was determined with the classic BET method (the Brunauer–Emmett–Teller isotherm). The BET isotherm is the basis for determining the extent of nitrogen adsorption on a given surface. A Micromeritics ASAP 2010 Chemisorption Surface Area Analyzer (Micromeritics Instrument Corp., Norcross, GA) was used in this work. Representative nanoparticle samples were pre-dried at room temperature (22±1 °C) in a vacuum desiccator and degassed at 90 °C for 1 h and then at 200 °C for 4 h. The iron sample was contained within a glass sample tube cooled to cryogenic temperature, then exposed to nitrogen gas at a series of precisely controlled pressures. With each incremental pressure increase, the number of nitrogen molecules on the surface increased. The pressure at which adsorption equilibrium occurs was measured and the universal gas law was applied to determine the quantity of gas molecules adsorbed. As adsorption proceeded, the thickness of the adsorbed nitrogen film increased with surface microspores being filled before macrospores. The process continued until the point of bulk condensation of the nitrogen and then the reverse sequence of desorption occurred. The systematic sorption and desorption of nitrogen provided the fundamental information on the surface characteristics—the total surface area.

2.2.4. X-ray diffraction

The method of X-ray diffraction (XRD) was used to investigate the material structure of iron nanoparticles. The XRD analysis was conducted with a Philips XRD 3100 diffractometer (Philips electronic Co., Eindhoven, Netherlands) at 45 kV and 30 mA. It used copper Kα radiation and a graphite

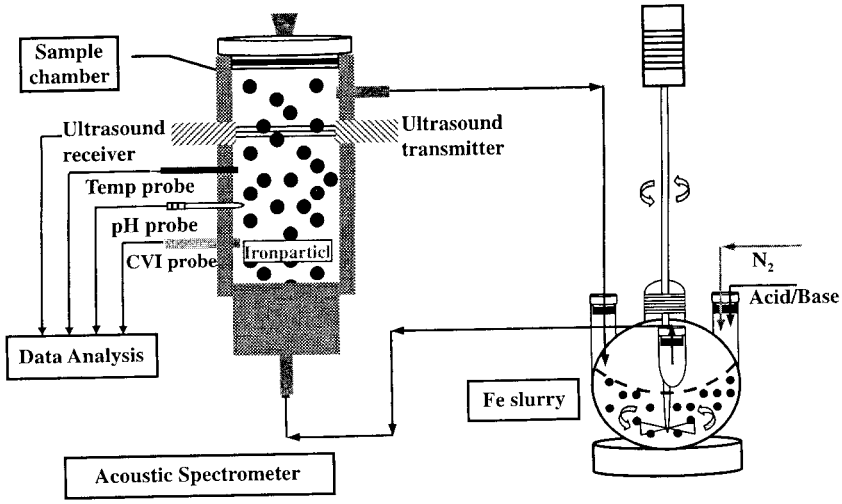

Fig. 2. Schematic of on-line nanoparticle characterization with acoustic spectrometer.

monochromator to produce X-rays with a wavelength of 1.54060 Å. Iron nanoparticles were placed in a glass holder and scanned from 20° to 60°. This scan range covered all major species of iron and iron oxides. The scanning rate was set at 2.0°/min.

2.2.5. X-ray photoelectron spectroscopy (XPS)

The use of this technique for iron nanoparticle analysis was mainly to determine the surface composition to a depth of less than 10 nm. In order to avoid further oxidation, the iron nanoparticle samples were prepared by drying in a small nitrogen-purged hood at room temperature and then packing into the sample cell directly. The analysis was conducted with a Scienta ESCA-300 high-resolution X-ray photoelectron spectrometer (HR-XPS). A Kα X-ray beam at 3.8 kW was generated from an Al rotating anode. The X-ray beam is monochromatized using seven crystals mounted on three Rowland circles. The kinetic energy was analyzed using a high-resolution 300-mm mean radius hemispherical electrostatic analyzer and detected by a multi-channel plate-CCD camera. The spectrum was obtained by plotting the measured photoelectron intensity as a function of the binding energy. The binding energies of the photoelectrons were calibrated by the aliphatic adventitious hydrocarbon C(1s) peak at 284.6 eV.

2.2.6. X-ray absorption near edge structure (XANES)

This technique uses synchrotron radiation to photo-ionize the core electrons of Fe atom and provides useful information on the valance of iron. When the increasing scanning energy is sufficient to eject the core electrons, the energy absorption abruptly increases (absorption edge). With the increasing oxidation state, the absorption edge shifts to higher energies and thus the valence state can be determined. XANES spectra of iron samples including metallic Fe, FeO, Fe_2O_3 and Fe_3O_4 were obtained on the Wiggler beamline at the Synchrotron Radiation Research Center (SRRC) in Hsinchu, Taiwan. The electron storage ring was operated with an energy of 1.3 GeV and a current of 100–200 mA. A Si(111) double-crystal monochromator (DCM) was used to provide highly monochromatized photon beams with energies of 1 to 9 keV and an energy resolution of 1.9×10^{-4} (eV/eV). The data were collected in transmission mode with a Lytle detector in the region of the Fe K edge (7112 eV) at room temperature. The absorption spectra were obtained using ion chambers filled with helium gas. The photon energy was calibrated with characteristic pre-edge peaks in the absorption spectrum of an iron foil. Each sample had four scans. The fractions of iron species in the samples were deduced using least-square fittings of the XANES spectra. The height and area of the near edge band in the iron spectrum are quantitatively proportional to the amount of Fe species. For the accuracy of data fitting, the residual of analysis was controlled within 3%.

2.2.7. ζ potential

The surface charge of iron nanoparticles is often characterized by the zeta (ζ) potential, which is defined as the electric potential at the surface of shear relative to that in the distant bulk medium. Surface charge or ζ potential is the major factor determining the mobility of particles in an electrical field. Measurement of ζ potential was carried out with the above-described electroacoustic method that detects the oscillation of charged particles in an acoustic field leading to the generation of an alternating electrical field and consequently to an alternating electric current (colloidal vibration current, CVI) for the determination of ζ potential. The detailed mechanisms and methods can be found elsewhere [31,32].

The magnitude and phase of the colloid vibration current is measured at 1.5 and 3 MHz. The CVI measurement at 1.5 MHz is used for determining only the CVI phase and correspondingly the sign of the ζ potential. At 3 MHz, the CVI measurement is used to determine the absolute value of the ζ potential. In addition, it is worthy to mention that the advantage of this instrument is no need of sample dilution, which usually influences the original surface charge.

2.2.8. Iso-electric point (IEP)

Titration of ζ potential versus pH was employed to determine the iso-electric point of iron nanoparticles. The experiment was conducted in the same setup showing in Fig. 2. The solution pH was adjusted with 2.0 N H_2SO_4 or 2.5 N NaOH through a manual syringe injection. A tunable mechanical stirring at a speed of 100 rpm was employed to achieve rapid mixing. During the experiment, the system was purged with high purity nitrogen gas. The titration began after the iron nanoparticles were suspended with DI water for 30 min to allow the solution to reach equilibrium, which may be judged from a gradually stable ζ potential.

2.2.9. pH/standard potential

1000 mL of nitrogen-purged distilled water was added to a Fernbach flask fitted with a customized rubber stopper containing ports for pH and redox potential electrodes and sampling. A variable speed mixer (Heindorf) set at 300 rpm helped to ensure well-mixed conditions. Measured dissolved oxygen levels were generally less than 0.1 mg/L after 30 min of N_2 purging. Then the iron nanoparticles were added.

A combination pH electrode (Orion) was used in conjunction with a Sension1 pH meter (Hach Co., Loveland, CO) to track solution pH and was calibrated prior to each test. A combination Ag/AgCl reference electrode (Cole-Parmer Instrument Co., Vernon Hills, IL) was used with a Model 420A pH/ORP meter (Allometrics, Inc., Baton Rouge, LA) to monitor standard potential and was calibrated with fresh ZoBell solution before each test. Measured redox potential readings (mV) were converted to Eh, the potential relative to the standard hydrogen electrode, as a function of solution temperature by adding +202 mV at 25 °C.

3. Results and discussion

Fig. 3 presents TEM images of the iron nanoparticles. The laboratory prepared iron particles were largely spherical,

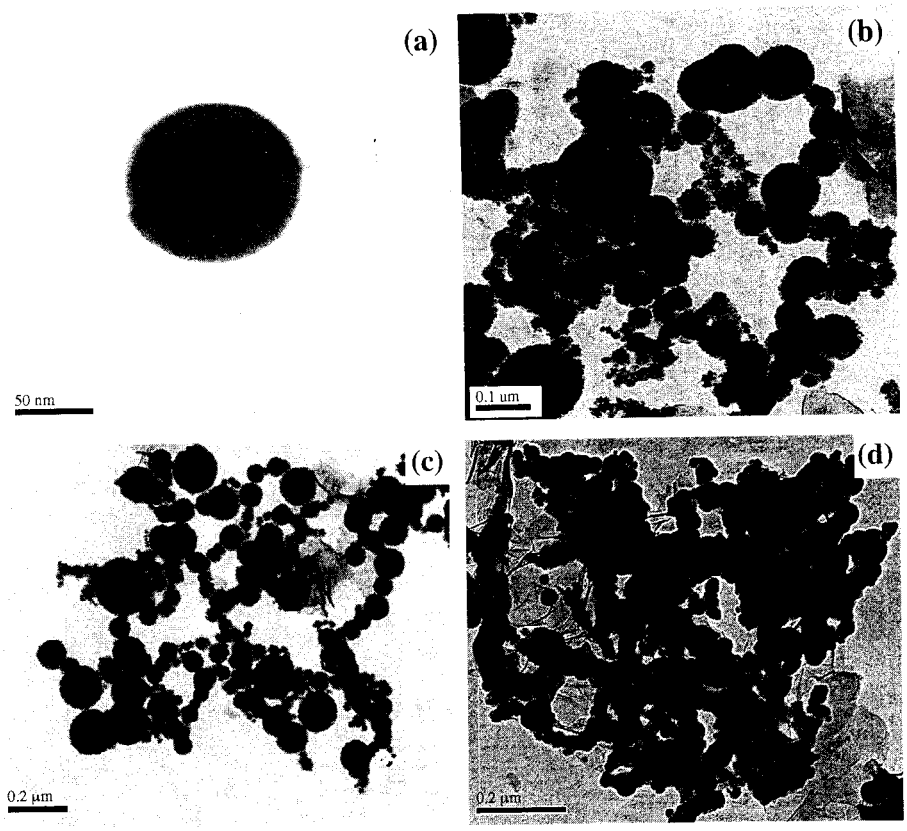

Fig. 3. Micrographs of: (a) a single particle and (b)–(d) aggregates of iron particles.

characteristic of particles formed in solution. A representative single particle size is around 60–70 nm as shown in Fig. 3a. A few particles had size as large as 200–250 nm, whereas most (>92%) particles were less than 100 nm. TEM images (Fig. 3b–d) also show that most particles formed chain-like aggregates.

A size distribution (Fig. 4a) was calculated after more than 420 particle TEM images were manually examined. The median size was around 60.2 nm, and average size 70.2 nm and standard deviation ~49.6 nm. Particle size and size distribution of the iron nanoparticles were further determined with the acoustic spectrometer. Fig. 4b contains a log-normal particle size distribution (PSD) of the synthesized iron particles. The density distribution (on *Y*-axis) is on the weight basis. The median diameter of iron nanoparticles was located at about 60.60 nm and the average (mean) size was ~105 nm, similar to the result from direct TEM observations presented in Fig. 3a. The slight difference between average sizes may be resulted from the missing of a few large particles (i.e., >300 nm) in the TEM samples. Nonetheless, both methods serve as complements in terms of quality assurance.

The iron nanoparticles have a rather broad PSD with a standard deviation of 0.421, which is defined as the ratio of size at 15.87% cumulative probability to that at 50% [32]. In other words, this work suggests that the chemically synthesized iron particles are polydisperse with a majority in the nano-domain (<100 nm). In general, particles can be called monodisperse if the standard deviation is less than <0.1.

For a spherical particle with a diameter of d, the specific surface area (SSA) can be calculated by the following equation:

$$\mathrm{SSA} = \frac{\text{Surface Area}}{\text{Mass}} = \frac{\pi d^2}{\rho \frac{\pi}{6} d^3} = \frac{6}{\rho d} \tag{2}$$

where ρ is the density (7800 kg/m^3 for iron) of the solid particle. The theoretical SSA for 60 nm particles is therefore 12,820 m^2/kg.

Three measurements with the BET surface area analyzer yielded SSA values in the range of 12,000–17,000 m^2/kg, with an average at 14,500 m^2/kg. The BET result suggested an average particle size around 53 nm. This slight deviation from the calculation may be caused by the density difference. As discussed late in this work, the surface iron was largely present as iron hydroxides. Thus, the true density of the nanoparticles in water would be slightly less than 7800 kg/m^3 for the metallic iron. In other words, the theoretical SSA should be higher than 12,820 /kg and may be closer to the measured value of 14,500 m^2/kg. As an experimental comparison, a 10–40-mesh (2–0.425 mm) iron filing from Aldrich was also analyzed. The Aldrich iron has a BET surface area of 1.5 m^2/kg, close (within 15%) to the surface area given by the supplier [34]. This was intended as a quality assurance and control for the BET method.

An example of the XRD spectrum of the nanoscale iron particles is shown in Fig. 5. The broad peak reveals the existence of an amorphous phase of iron. Apparent peaks at the 2θ of 44.9° and 35.8° indicate the presence of both zero-valent

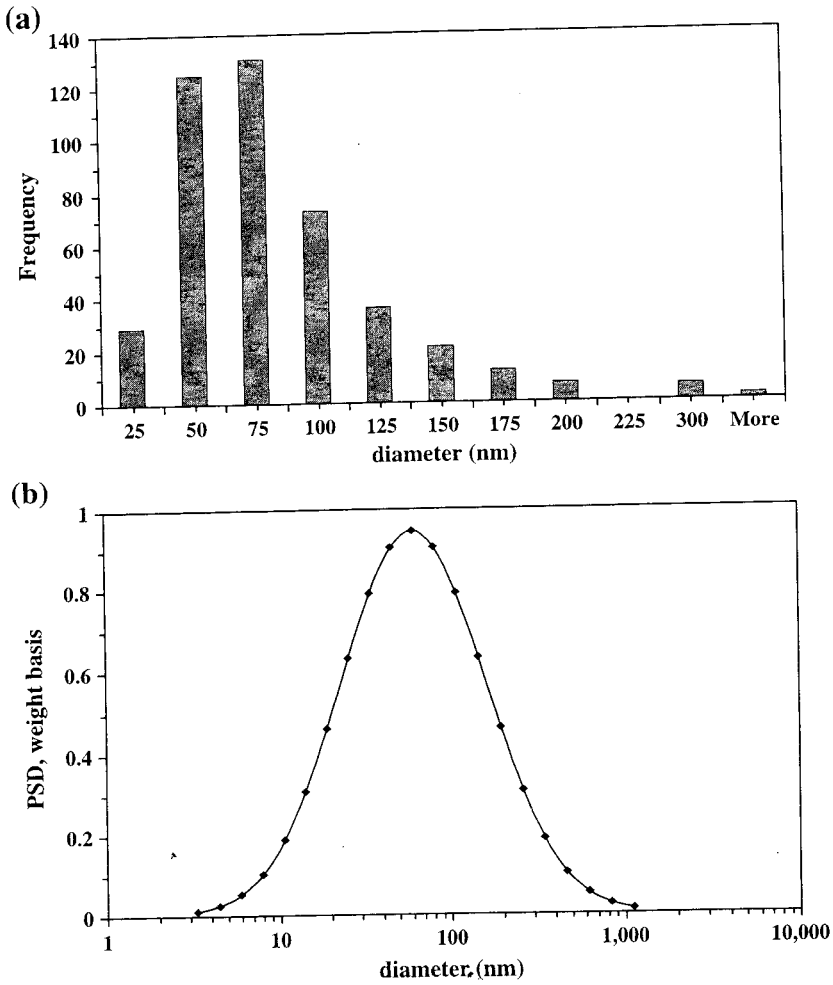

Fig. 4. Particle size distribution (PSD) of zero-valent iron nanoparticles. (a) TEM method. The median diameter is located at 60.2 nm. (b) Ultrasonic method. The median diameter is located at 60.6 nm.

iron (α-Fe) and iron oxide (FeO) crystalline phases. This was further confirmed by the XPS response (Fig. 6). Fig. 6a shows a full survey of the surface composition. No major change was observed from 3-h and 24-h samples. Little boron (B) was detected on the iron surface. For the survey of Fe 2p core levels (Fig. 6b), the photoelectron peaks at 710.56 eV, 719.26 eV and 723.91 eV represent the binding energies of Fe($2p_{3/2}$), shake-up satellite $2p_{3/2}$ and $2p_{1/2}$, respectively. The three main feature peaks suggest that the surface of iron nanoparticles consist mainly of a layer of iron oxides, likely in the form of FeO [35]. Furthermore, a small shoulder at around 706.01 eV can also be observed, suggesting the $2p_{3/2}$ peaks of zero-valent iron (Fe^0).

The XANES spectrum of aged (>3 weeks) iron particles is shown in Fig. 7. The fitting results suggest about 44% of zero-

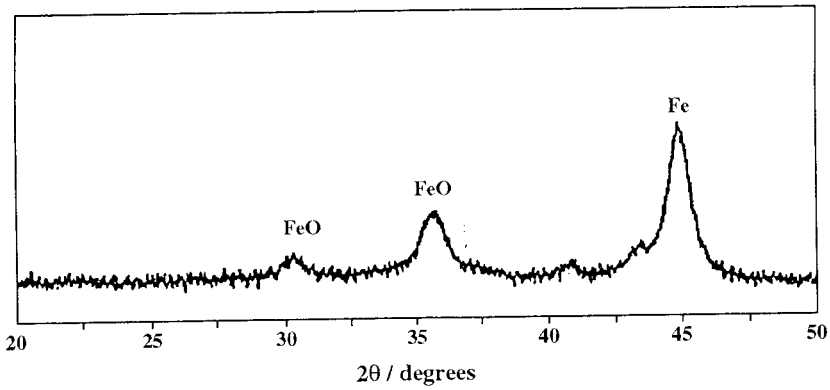

Fig. 5. X-ray diffractogram of the synthesized iron nanoparticles.

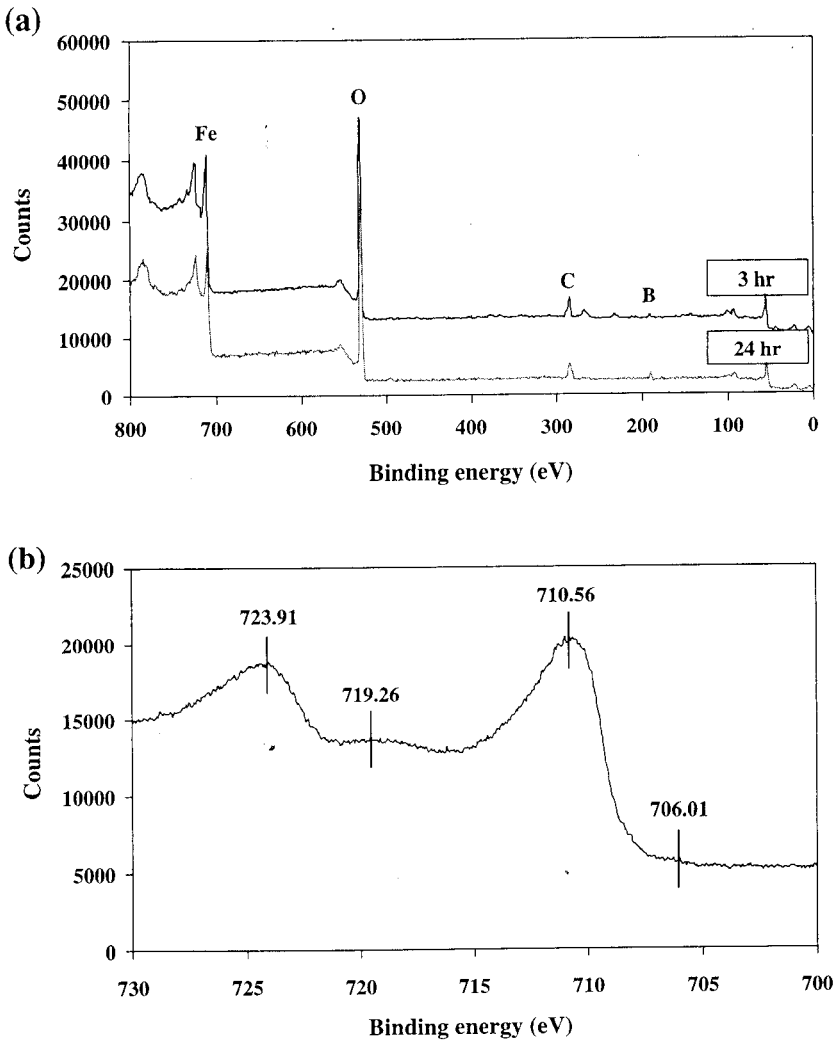

Fig. 6. XPS response of (a) full survey and (b) Fe 2p core levels of iron nanoparticles.

valent iron and 56% FeO in the iron sample. Interestingly, no Fe (III) was observed. For fresh iron particles, the fraction of the zero-valent iron is supposed to be higher (>80%). From the combined results of XRD, XPS and XANES, it can be concluded that the iron nanoparticles likely have a core of main zero-valent iron (Fe^0), while a shell is largely made of iron

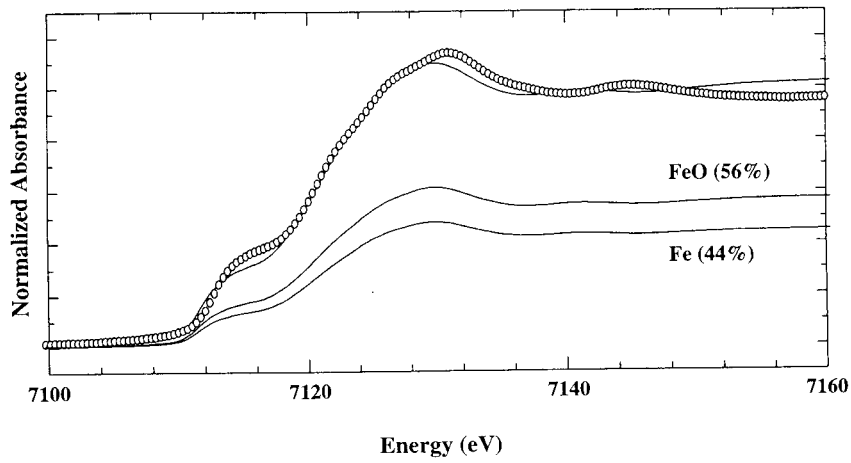

Fig. 7. XANEs spectra of iron particles and the least-square fitting result, suggesting 44% of zero-valent iron and 56% of FeO for a 3-week-old sample.

oxides (i.e., FeO). In aqueous solution, as a result of surface hydroxylation [36], the surface is likely in the form of FeOOH. These results are in general consistent with reported work suggesting a core-shell structure for the iron nanoparticles [37,38].

The hydrated surface may also give raise to the surface charge in water. The impact of solution pH on surface charge is typically characterized by iso-electric point (IEP), the critical pH value at which the net surface charge is zero. Fig. 8 shows the ζ potential of the iron nanoparticles as a function of solution pH. IEP was found to be near pH $\approx$ 8.3. Even for aged (>1 month) iron particles, variation or shift of IEP was not observed, likely due to a nearly oxidized or stabilized surface of as-synthesized iron particles. Thus, further oxidation of the core may be considered having limited influence on the surface characteristic (i.e., IEP). Comparatively, IEP of iron nanoparticles is higher than that of magnetite (Fe_3O_4) (~6.8) or maghemite (γ-Fe_2O_3) (~6.6) [36].

The IEP value is apparently independent of nanoparticle concentrations as shown in Fig. 8. However, it shifted with the addition of an inert electrolyte (KCl), suggesting the adsorption of chloride ion on iron surface. In general, anions, such as chloride and phosphate, may serve as ligands because they have one or more atoms with a lone pair of electrons and can function as the donor in a coordinate bond. Iron nanoparticles have an outside iron oxide surface where ligands may be adsorbed either specifically (Eqs. (3) and (4)) or non specifically (Eq. (5)) [36]:

$$\equiv FeOH + L^- \leftrightarrow \equiv FeL + OH^- \quad (3)$$

$$\equiv (FeOH)_2 + L^- \leftrightarrow \equiv Fe_2L^+ + 2OH^- \quad (4)$$

$$\equiv FeOH + L^- + H^+ \leftrightarrow \equiv Fe(OH)_2^+L^- \quad (5)$$

where the symbols $\equiv$ and L^- represent the iron surface and anion ligands, respectively. The adsorption of anions decreases IEP because more protons, i.e., more acid, are needed to neutralize the negative charge of the adsorbed anions [39].

The surface charge or ζ potential of the iron nanoparticles may have important implication on their suspension stability and mobility in soil and groundwater environment. Aquifer materials generally have universal negative surface charges in the neutral pH range. Hence, the iron nanoparticles with positive charges at pH lower than 8.3 are attractive to aquifer materials. This may explain the apparent aggregation of the synthesized iron nanoparticles and also relatively low mobility in porous media (e.g., sand column or aquifer).

Zero-valent iron, Fe^0, has long been recognized as an effective electron donor regardless of its particle size. This is evidenced by the standard reduction potential (E^0) of −440 mV for the following half-reaction between the Fe^{2+}/Fe^0 couple:

$$Fe^{2+} + 2e^- \rightarrow Fe^0. \quad (6)$$

In the subsurface environment, the predominant electron receptors are water and to some extent residual dissolved oxygen:

$$Fe^0_{(s)} + 2H_2O_{(aq)} \rightarrow Fe^{2+}_{(aq)} + H_{2(g)} + 2OH^-_{(aq)} \quad (7)$$

$$2Fe^0_{(s)} + 4H^+_{(aq)} + O_{2(aq)} \rightarrow 2Fe^{2+}_{(aq)} + 2H_2O_{(l)} \quad (8)$$

According to the above reactions, these zero-valent iron-mediated redox reactions should produce a characteristic increase in solution pH and a concomitant decline in solution potential (Eh). As suggested in Eq. (7), the dissociative adsorption of water on the iron surface results in the formation of surface-bound hydroxyl species. Given its overwhelming concentration advantage as the solvent, the reduction of water at the iron surface can be expected to be the dominant redox process in the system. In other words, a highly reducing condition is expected with the presence of iron nanoparticles.

Fig. 9 presents the observed pH and Eh trends for a relatively simple system containing only nanoscale iron particles

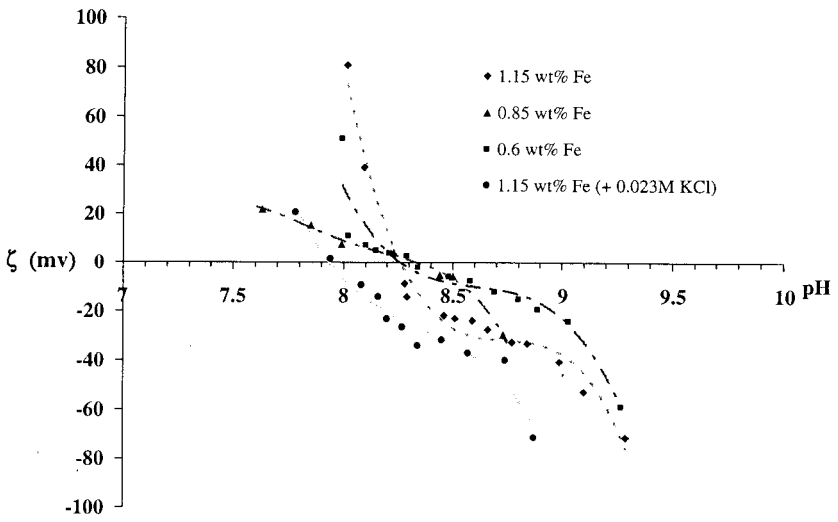

Fig. 8. ζ potential as a function of solution pH.

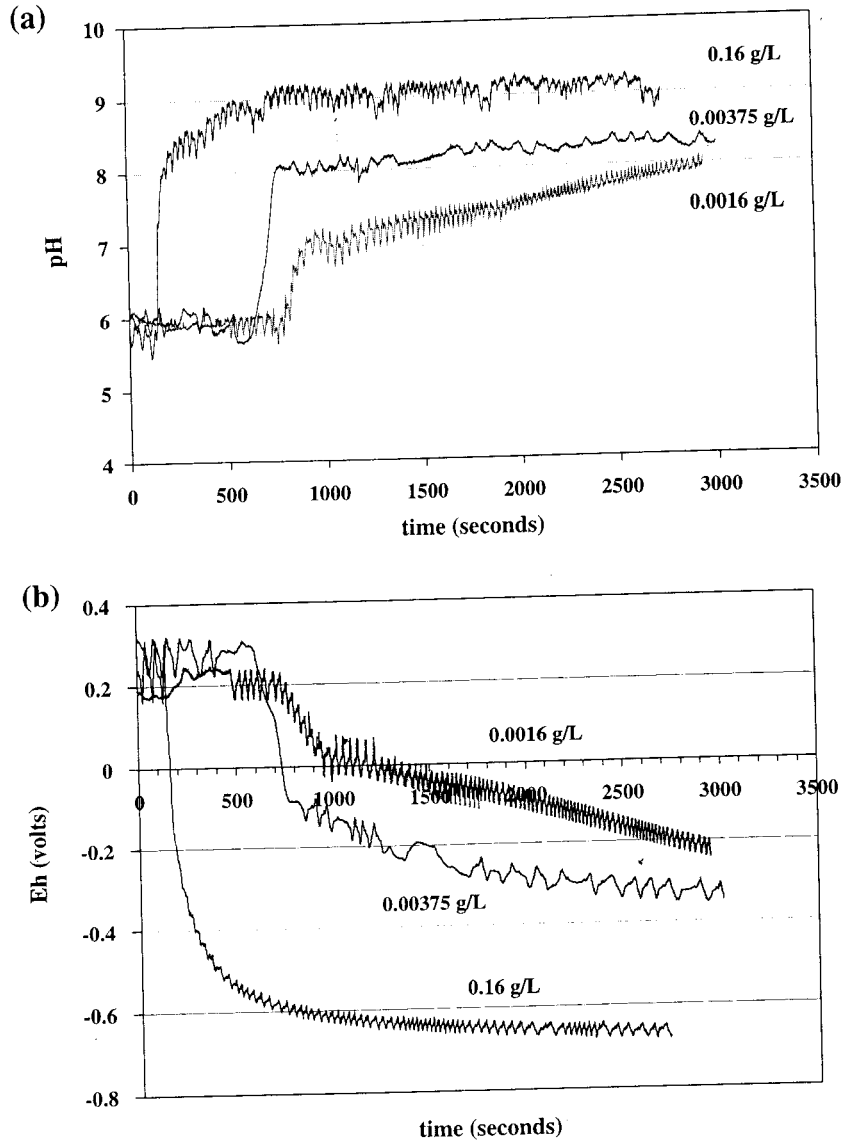

Fig. 9. pH and Eh trends as functions of reaction time and iron nanoparticle concentration.

suspended in distilled water. Our experiments showed a typical increase in pH of approximately 2–3 standard units from pH ~ 6 to 8–9. Even with excessive iron nanoparticles (>10 g/L, data not shown), the equilibrium pH was less than 10. The pH upsurge is expected to be much smaller in well-buffered and flowing groundwater. A corresponding precipitous decline in solution Eh from +400 mV to approximately −500 mV was observed. Due to the large reactive surface and rapid reactions, 2–3 mg/L of iron nanoparticles was sufficient to achieve a negative Eh solution in a relatively short time (<1 h).

The ability of iron nanoparticle to rapidly reduce groundwater redox potential may prove not only vital for chemically induced degradation of contaminants but also potentially useful for stimulating reductive biodegradation of chlorinated solvents. The addition of trace amounts of iron nanoparticles quickly reduces the standard potential, generates hydrogen gas and produces divalent iron. These conditions are naturally favorable for the growth of anaerobic microorganisms.

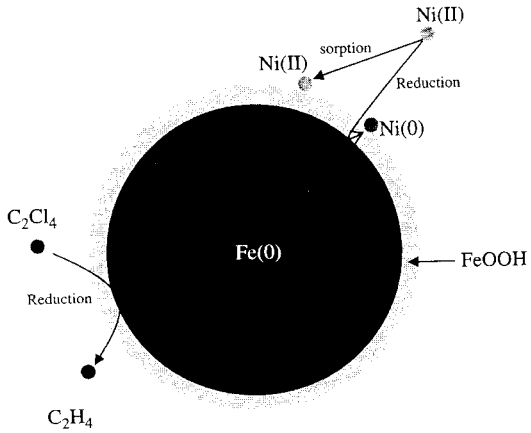

Fig. 10. A core-shell structure for iron nanoparticles in aqueous solution. The core is made of metallic iron while the shell consists mostly of iron oxides and hydroxides. Thus iron nanoparticles exhibit characteristics of both iron oxides (e.g., as a sorbent) and metallic iron (e.g., as a reductant).

A conceptual model of the iron nanoparticles is illustrated in Fig. 10. As shown in this work, the iron nanoparticles exhibit the dual characteristics of iron hydroxides (i.e., complex formation) and of zero-valent iron (i.e., reduction). The adsorption properties of iron oxides in aquatic systems have been extensively documented [40,41]. In water, iron oxides can have metal-like or ligand-like coordination properties depending on the solution chemistry (e.g., pH). At low pH, iron oxides are positively charged and attract negatively charged ligands (e.g., phosphate). When solution pH is above the iso-electric point (pH = ~8), the oxide surface becomes negatively charges and can form surface complexes with cations (e.g., Ni(II)). When sufficient (e.g., >0.1 g/L) iron nanoparticles are added to water, solution pH is typically in the range of 8–10.

4. Conclusions

Iron nanoparticles synthesized with the borohydride method have been characterized with the techniques of TEM, XRD, HR-XPS, XANES, acoustic spectrometer and BET nitrogen adsorption isotherm. Average particle size of the particles is approximately 60 nm with majority (>90%) in the nano-domain (1–100). Iso-electric point (IEP) is in the range of pH 8.1–8.3. The nanoparticles have strong tendency to form microscale aggregates likely due to the weak surface charges. In water, 2–3 mg/L iron loading is sufficient to achieve a negative oxidation–reduction potential. Iron nanoparticles have a core of zero-valent iron and a shell of mainly iron oxides (FeO). The dual properties of iron nanoparticles may prove to be useful for the separation and transformation of many contaminants and worth to be studied more systematically.

Acknowledgements

This research is partially supported by USEPA STAR grants (R829624 and GR832225).

References

[1] Brumfiel G. Nature 2003;424:246.
[2] Mohamed H, Hassan A. Science 2005;309:65.
[3] Zhang W. J Nanopart Res 2003;5:323.
[4] Wang C, Zhang W. Environ Sci Technol 1997;31:2154.
[5] Mahfuz U, Ahmed M. Sci Technol Adv Mater 2005;6:302.
[6] Rose-Pehrsson S, Pehrsson P. Nanotechnology and the environment. Washington, DC: American Chemical Society; 2005.
[7] Abrams B, Wilcoxon J. Crit Rev Solid State 2005;30:153.
[8] Yuan G. J Environ Sci Health 2004;39:2661.
[9] Nagaveni K, Sivalingam G, Hegde S, Madras G. Environ Sci Technol 2004;38:1600.
[10] Modi A, Koratkar N, Lass E, Wei B, Ajayan P. Nature 2003;424:171.
[11] Karlsson A, Deppert K, Wacaser A, Karlsson S, Malm O. Appl Phys A Mater 2005;A80:1579.
[12] Choi Ch, Dong X, Kim B. Mater Trans 2001;42:2046.
[13] Elihn K, Otten F, Boman M, Kruis F, Fissan H, Carlsson J. Nanostruct Mater 1999;12:79.
[14] Glavee GN, Klabunde KJ, Sorensen CM, Hadjipanayis GC. Inorg Chem 1995;34:28.
[15] Khalil H, Mahajan D, Rafailovich M, Gelfer M, Pandya K. Langmuir 2004;20:6896.
[16] Xu J, Dozier A, Bhattacharyya D. J Nanopart Res 2005;7:449.
[17] Zhang W, Wang C, Lien H. Catal Today 1998;40:387.
[18] Schrick B, Blough J, Jones A, Mallouk T. Chem Mater 2002;14:5140.
[19] Elliott D, Zhang W. Environ Sci Technol 2001;35:4922.
[20] Kroschwitz J, Howe-Grant M. Encyclopedia of chemical technology. 4th ed. New York: Wiley & Sons; 1993.
[21] Nutt M, Hughes J, Wong M. Environ Sci Technol 2005;39:1346.
[22] Doyle J, Miles T, Parker E, Cheng I. Microchem J 1998;60:290.
[23] Elliott D, Cao J, Zhang W, Spear S. The 225th ACS National Meeting, New Orleans, LA, United States, vol. 43; 2003. p. 564.
[24] He F, Zhao DY. Environ Sci Technol 2005;39:3314.
[25] Liu YQ, Majetich SA, Tilton RD, et al. Environ Sci Technol 2005; 39:1338.
[26] Alowitz M, Scherer M. Environ Sci Technol 2002;36:299.
[27] Cao J, Elliott D, Zhang W. J Nanopart Res 2005;7:499.
[28] Kanel S, Manning B, Charlet L, Choi H. Environ Sci Technol 2005;39:1291.
[29] Glazier R, Venkatakrishnan R, Gheorghiu F, Walata L, Nash R, Zhang W. Civ Eng 2003;73:64.
[30] Quinn J, Geiger C, Clausen C, Brooks K, Coon C, O'hara S, et al. Environ Sci Technol 2005;39:1309.
[31] Dukhin AS, Goetz PJ, Truesdail S. Langmuir 2001;17:964.
[32] Dukhin AS, Goetz PJ. Ultrasound for characterizing colloids: particle sizing, zeta potential, rheology. New York: Elsevier Science; 2002.
[33] Morrison ID, Ross S. Colloidal dispersions: suspensions, emulsions, and foams. New York: John Wiley & Sons; 2002.
[34] Cao J, Clasen P, Zhang W. J Mater Res 2005;20:3238.
[35] Allen GS, Curtis MT, Hooper AJ, Tucker PM. JCS Dalton 1974;14:1525.
[36] Cornell RM, Schwertmann U. The iron oxides: structure, properties, reactions, occurrences, and uses. 2nd ed. Weinheim: Wiley-VCH; 2003.
[37] Nurmi JT, Tratnyek PG, Sarathy V, Baer DR, Amonette JE, Pecher K, et al. Environ Sci Technol 2005;39(5):1221.
[38] Liu Y, Choi H, Dionysiou D, Lowry GV. Chem Mater 2005;17:5315.
[39] Otterstedt J, Brandreth DA. Small particles technology. New York: Plenum Press; 1998.
[40] Dzombak DA, Morel FMM. Surface complexation modeling. Wiley-Interscience; 1990.
[41] Stumm W. Chemistry of the solid–water interface. Wiley-Interscience; 1992.